

Multidimensional visual field maps: Relationships among local psychophysical and local electrophysiological measures

William Seiple, PhD; Karen Holopigian, PhD; Janet P. Szlyk, PhD; Carolyn Wu, MD

Department of Ophthalmology, New York University School of Medicine, New York, NY; Chicago Department of Veterans Affairs (VA) Health Care System, West Side Division, Chicago, IL; Department of Ophthalmology and Visual Sciences, University of Illinois at Chicago, Chicago, IL

Abstract—Multidimensional psychophysical and electrophysiological maps of the central retina are essential for assessing the functioning of the diseased retina. In this study, grating acuity, contrast sensitivity, duration for letter identification, multifocal electroretinograms, and Humphrey visual field thresholds were measured at equivalent positions throughout the central 20°. We found that the rates of sensitivity loss were not equivalent for all psychophysical measures. The rate of loss in the duration required for letter identification as a function of eccentricity was the steepest, followed by acuity and contrast sensitivity. The rate of loss in luminance sensitivity as measured in the Humphrey visual field was the shallowest. The pattern of losses also varied across meridians. Specifically, the rate of loss as a function of eccentricity was highest in the vertical meridian and lowest in the horizontal meridian. These maps and the correlations among measures as a function of retinal position serve as a baseline so that we can examine disease effects throughout the retina. In addition, the development of vision rehabilitation programs focused on eccentric viewing training should consider the differential sensitivities of the peripheral retina.

Key words: acuity, contrast sensitivity, eccentricity, electroretinogram.

INTRODUCTION

Retinotopic maps of luminance sensitivity derived from visual field testing (e.g., Humphrey visual fields) are widely accepted clinical measures of disease effects

on vision. A method of obtaining corresponding electrophysiologic maps of retinal function derived from the multifocal electroretinogram (mfERG) has been broadly applied [1–3]. However, the manner in which these maps relate to the complex psychophysical abilities of the peripheral retina has not been examined. Multidimensional mapping of the functional capabilities of the healthy visual system is an important starting point for understanding the perceptual consequences of visual diseases. For example, one might measure a visual acuity of 20/100 (logMAR equivalent = 0.7) in a central vision loss patient who uses an eccentric fixation locus at 10° in

Abbreviations: asbs = apostilb, CCD = charge-coupled device, CRT = cathode ray tube, EDI = electronic document interchange, LED = light-emitting diode, mfERG = multifocal electroretinogram, PRL = preferred retinal location, VA = Department of Veterans Affairs.

This material was based on work supported by a grant from the U.S. Department of Veterans Affairs, a center grant from The Foundation Fighting Blindness, the Allene Reuss Foundation, and an unrestricted grant from the Research to Prevent Blindness Foundation to the Department of Ophthalmology, New York University School of Medicine.

Address all correspondence to William Seiple, PhD; Department of Ophthalmology, New York University School of Medicine, 550 First Avenue, New York, NY 10016; 212-263-6076; fax: 212-263-8749; email: whs4@nyu.edu.

the temporal retina. An interesting question arises: Does 20/100 represent normal acuity for this eccentric location? A map of normal acuity as a function of retinal location is essential to answer this question, and multidimensional maps are required to fully characterize normal eccentric visual function.

Functional field maps could also be used to calculate the impact of functional field losses on orientation and mobility. In addition, they are an essential tool for assessing the outcomes of vision rehabilitation efforts, and local surgical, medical, or biomedical interventions. If acuity at a preferred retinal location (PRL) improves because of intervention, one might wish to know whether the amount of improvement returns performance to the level of control subjects for that retinal locus.

For example, if one observes an acuity improvement from 20/400 (logMAR equivalent = 0.7) to 20/100 at the fovea, or a similar improvement from 20/400 to 20/100 at a location that is 10° in the periphery, where did the intervention have the optimal effect? Since we know that acuity in the fovea is better than 20/20 in control patients, the treatment, although having some effect, did not return visual function to a “normal” level. From our present data, visual acuity at 10° would be expected to be approximately 20/100; therefore, the same magnitude of recovery (from 20/400 to 20/100) represents a return to normal vision and the optimum improvement that could be expected. Unless maps of visual function for control subjects are available, this sort of analysis could not be done. To apply this analysis to any study group, we must collect the same sort of data from age-matched control subjects. However, we do not foresee that complete maps would be collected for every patient. In patients, visual function could be assessed only in the areas of the retina that are of interest. The need for multidimensional psychophysical field maps of normal function is underscored by evidence suggesting that unitary relationships between losses of the underlying retinal integrity and losses of visual psychophysical performance [4–6], or between local losses of Humphrey visual field sensitivity and local mfERG losses, are not expected [7].

Much work exists describing the changes in the temporal and spatial resolution of the cone system as a function of eccentricity [8–17]. Relatively little work has examined eccentricity-dependent visual performance for psychophysical tasks at more than one meridian [13,18–21]. In the study, we mapped acuity, contrast sensitivity, and temporal sensitivity as a function of retinal eccentricity

and meridian. We then compared the psychophysical data to local electrophysiological responses and to Humphrey visual field thresholds obtained from the same subjects.

METHODS

Subjects

Four normally sighted, healthy adults (ages 24, 28, 40, and 49) gave informed consent to participate in this study. All subjects were trained psychophysical observers. The subjects' eyes were refracted to $\geq 20/20$ (logMAR = 0) central acuity. Each subject was tested monocularly, using his or her right eye. The research followed the tenets of the Declaration of Helsinki. The New York University institutional review board approved the research protocol.

Visual targets

Targets were presented on an Apple 12-inch monochrome monitor (67 Hz frame rate). Mean background luminance was 46 cd/m² and target luminance was 73 cd/m². A white foam board surrounded the monitor and was illuminated to the same mean luminance as the screen. Changing fixation locations allowed targets to be presented along eight meridians: horizontal—0° and 180°, vertical—90° and 270°, and oblique—45°, 135°, 225°, and 315°.

Procedures

The subject's left eye was patched and his or her head placed in a forehead and chin rest to minimize movement. To reduce eye movements during target presentation, the subject was instructed to fixate on an illuminated light-emitting diode, or LED (mean luminance = 50 cd/m²). On each trial, the LED either flickered (25 Hz, 50% modulation) simultaneously with the presentation of a peripheral target, or did not flicker. The subject stated whether or not the LED flickered and then identified the peripheral target. A similar method to activate ensure fixation was used by Seiple et al. [22] and by Regan and Beverley [18]. In addition, we used a CCD (charge-coupled device) camera to monitor the position of the pupil during stimulus presentation. With this monitoring system, saccades 1° or greater were readily apparent. Only trials with steady fixation and correct LED responses were accepted to ensure that the targets always fell at the intended retinal position. A “white” noise screen that controlled the physical duration of the stimulus followed the target presentation. The

order of the testing procedure was (1) a 500 ms warning tone, (2) the fixation LED either flickered or not and simultaneously a target was presented in the peripheral retina, (3) a “white” noise screen was presented for 750 ms, (4) the subject stated whether the LED flickered and identified the target seen in the periphery. The subject was required to guess when he or she felt uncertain and was not given feedback concerning the accuracy of the response.

Threshold Procedure

In Experiments I, II, and III, the dependent variable was target size, target contrast, and target duration, respectively. Size, contrast, and duration were controlled with the use of a “3 down/1 up” staircase procedure; that is, the target value was decreased after three consecutive correct responses, but was increased after one incorrect response. The run continued until nine reversals of the staircase were obtained. The software controlled the value of the step size: for the first two reversals, the step size was large; for the next three reversals, the step size was intermediate; and, for the final four reversals, the step size was the smallest available. The values of the final four reversals of the staircase were averaged to determine the threshold. The impact of the number of response choices on the psychometric function has been discussed by Seiple et al. [22]. Increasing the number of choices results in small and constant threshold elevation that does not vary with eccentricity, or with meridian.

Multifocal ERG

Stimulus. The mfERG technique used in this study was based on the work of Sutter and Tran [1], and our methods have been described in detail in Hood et al. [23]. The stimulus was an array of 103 hexagons, scaled in area to produce approximately equivalent mfERG amplitudes as a function of eccentricity. At the viewing distance of 32 cm, the entire array subtended 47° horizontally by 39° vertically. The stimulus array was generated on a black and white monitor (Nortec, 75 Hz frame rate) by means of a customized Macintosh video card (EDI, or electronic data interchange). The luminance of the white and black hexagons was 275 and 2 cd/m², respectively.

Recording Technique. Following pupil dilation (1.0% tropicamide and 2.5% phenylephrine hydrochloride), we anesthetized the cornea (0.5% proparacaine). We recorded responses from the right eye using a bipolar Burian-Allen contact lens electrode (Hansen Ophthalm-

ics, Iowa City, IA) with the ipsilateral earlobe used as a ground. The left eye was patched. A corrective lens provided the subject with best-corrected acuity for the viewing distance. We calculated response density in $\eta v^{\circ 2}$ for each hexagon using the VERIS software.

Humphrey Visual Field

Threshold visual fields were measured from the subject’s right eye using a Humphrey Visual Field Analyzer. The right eye was refracted for the viewing distance and the left eye was patched. The test spots subtended 0.43° and were presented for 200 ms. Positions of the test spots were modified to correspond to the centers of the hexagons in the mfERG array.

RESULTS

Experiment I. Grating Acuity

Procedures

Gratings were presented for 50 frames at 63 percent contrast and grating bar widths ranged from 0.9 to 9.0 minarc. Two and one-half cycles of the grating were shown at each target size. On each trial, the orientation of the grating was randomly chosen to be either horizontal or vertical. The subject fixated on the LED, responded whether it flickered, and stated the orientation of the grating. Spatial frequency of the grating was controlled by the staircase procedure just described.

Results

The median (N = 4) thresholds (in minarc) are plotted as a function of eccentricity for each of the eight meridians in **Figure 1(a)**. For all meridians, the bar width needed to discriminate the orientation of a grating increased with increasing eccentricity. The data for each meridian were best-fitted by the exponential equation

$$y = A_0 + \exp(A_1 x) \quad (1)$$

where A_0 is the intercept, and A_1 is the slope that determines the rate of acuity loss as a function of eccentricity. The values of the parameters of the fits are presented in **Table 1**. Grating acuity peaked at fixation and showed a fall-off with eccentricity, with A_1 averaging 0.12 across all meridians. The rate of acuity loss with increasing eccentricity was less along the horizontal meridians (0°

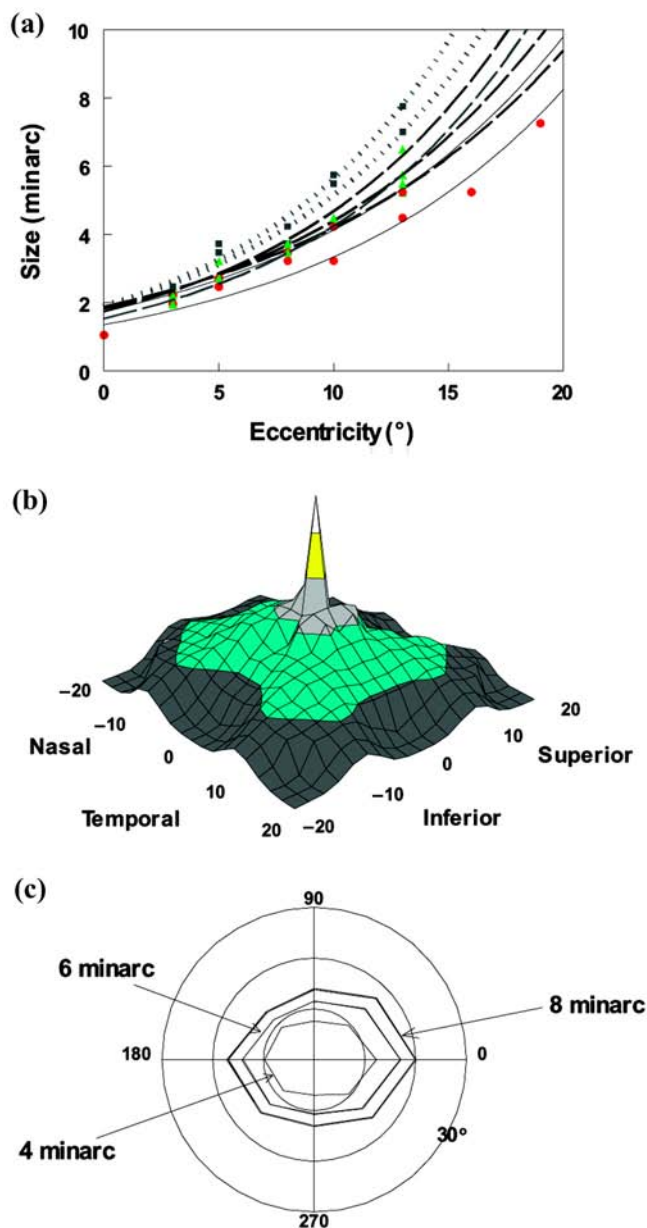


Figure 1.
Grating Contrast. (a) Threshold grating width is plotted against eccentricity for 8 meridians: horizontal—0° and 180° (solid lines/filled circles); vertical—90° and 270° (broken lines/squares); and oblique—45°, 135°, 225°, and 315° (dashed lines/triangles). (b) 3D plot of sensitivity (1/acuity threshold) derived from data presented in (a). Lighter areas represent regions with higher sensitivity. (c) Isoacuity plots derived from data presented in (a).

and 180°) than along the vertical meridians (90° and 270°) (Figure 1(a)). Oblique meridians (45°, 135°, 225°, and 315°) showed intermediate rates of loss.

Using the data presented in Figure 1(a), we derived threshold acuities as a function of eccentricity and meridian, and these data were plotted as a 3D (three-dimensional) plot of sensitivity (1/acuity threshold) in Figure 1(b). There was a sharp peak in sensitivity at fixation, with a decline with increasing eccentricity. Isoacuity contours were also calculated from these data. For each meridian, we determined the most eccentric point at which a grating of a given size (4-, 6-, and 8-minarc bar width) was discriminated. We joined these points to create Figure 1(c), which further quantifies the eccentricity-dependent acuity loss as a function of meridian. Sensitivity was elongated in the horizontal relative to the vertical meridian. For example, gratings with a bar width of 8 minarc were detected to approximately 18° eccentricity horizontally and approximately 13° vertically.

Experiment II. Grating Contrast Sensitivity

Procedures

Square wave gratings were presented within a 32 minarc window. Two-and-one-half cycles of the grating were shown in the window (bar width of 6.4 minarc) for a duration of 50 frames. On each trial, the orientation of the grating was randomly chosen to be either horizontal or vertical. The subject fixated on the LED, responded whether the LED flickered, and stated the orientation. The subject was required to guess when the orientation could not be discriminated. Grating contrast was controlled over a range between 1.9 percent and 58.0 percent by the staircase procedure described previously.

Results

Median ($N = 4$) contrast thresholds are plotted as a function of eccentricity for each meridian in Figure 2(a). For all eight meridians, the contrast required to discriminate the orientation of the grating increased with increasing eccentricity. The rate of contrast sensitivity loss was less along the horizontal meridians than along the vertical meridians. Once again, oblique meridians showed intermediate rates of contrast sensitivity loss. A 3D plot of contrast sensitivity (1/contrast threshold) is shown in Figure 2(b). Grating contrast sensitivity peaked at fixation and demonstrated a steeper fall-off with eccentricity (average $A_1 = 0.42$) than did acuity. The rate of sensitivity decline was not symmetrical with meridian. The iso-contrast contour plot (Figure 2(c)) demonstrates the range of eccentricities and the variations as a function of meridian over which orientation of gratings of a given

Table 1.
Fit results.

Test	0°	45°	90°	135°	180°	225°	270°	315°
Acuity								
A_0	0.99	1.08	1.15	1.04	0.93	0.93	1.25	0.78
A_1	0.10	0.11	0.14	0.12	0.11	0.13	0.14	0.12
r^2	0.99	0.97	0.96	0.97	0.99	0.97	0.98	0.97
Contrast								
A_0	-4.10	-1.13	-15.10	-5.80	-2.43	-4.71	-18.55	-8.97
A_1	0.24	0.46	0.53	0.41	0.30	0.41	0.52	0.45
r^2	0.95	0.99	0.95	0.85	0.92	0.94	0.92	0.96
Letter Identification								
A_0	-4.44	-1.13	-15.10	-5.80	-2.44	-4.77	-16.10	-10.23
A_1	0.27	0.46	0.53	0.41	0.30	0.41	0.52	0.47
r^2	0.98	0.99	0.97	0.85	0.92	0.94	0.94	0.96
mfERG								
A_0	-0.96	-0.95	-0.95	-0.95	-0.96	-0.95	-0.94	-0.95
A_1	0.007	0.009	0.009	0.008	0.008	0.008	0.009	0.010
r^2	0.99	0.96	0.97	0.95	0.99	0.94	0.94	0.99
Humphrey								
A_0	2.68	4.39	4.30	3.33	2.52	3.91	4.05	4.63
A_1	0.12	0.10	0.11	0.09	0.09	0.09	0.08	0.15
r^2	0.94	0.87	0.95	0.85	0.93	0.90	0.77	0.96

contrast (10%, 20%, and 40%) were discriminated. At equivalent eccentricities, sensitivities were higher along the horizontal than along the vertical meridians.

Experiment III. Duration for Letter Identification

Procedures

A set of nine Sloan letters was chosen (D, H, K, N, O, R, S, V, and Z). Overall target size was 32 minarc, and we drew the letters using stroke widths of one-fifth of the overall target window. The mean background luminance was 46 cd/m², and the letter luminance was 73 cd/m² (Weber contrast = 0.59). On each trial, we presented a letter chosen randomly from the set of nine letters. The subject fixated on the LED, responded whether the LED flickered, and named the letter. The staircase algorithm controlled the duration of the letter presentation. Since a cathode-ray tube (CRT) was used to present the stimuli, all the duration threshold results were presented in number of frames (at a frame rate of 67 Hz, each frame was nominally 15 ms).

Results

The median ($N = 4$) threshold durations (in frames) for letter identification are plotted as a function of meridian and eccentricity in **Figure 3(a)**. The duration required to identify letters increased with increasing eccentricity at all meridians. The values of the fits of equation (1) to these data are listed in **Table 1**. These data were then used to derive temporal detection sensitivities as a function of eccentricity and meridian. The results are plotted in **Figure 3(b)**. Temporal sensitivity peaked at the center and decreased as a function of eccentricity. Again, the rate of sensitivity decline was not symmetrical as a function of meridian showing higher sensitivities along the horizontal than along the vertical meridians for equivalent eccentricities. The isoduration contour plot (**Figure 3(c)**) shows the range of eccentricities and the variations as a function of meridian, over which letters presented at a particular duration (125, 250, and 500 ms) were identified. For example, 32 minarc letters (bar width of 6.4 minarc) presented at a duration of 125 ms were detected out to a maximum of 17° horizontally and 9° vertically.

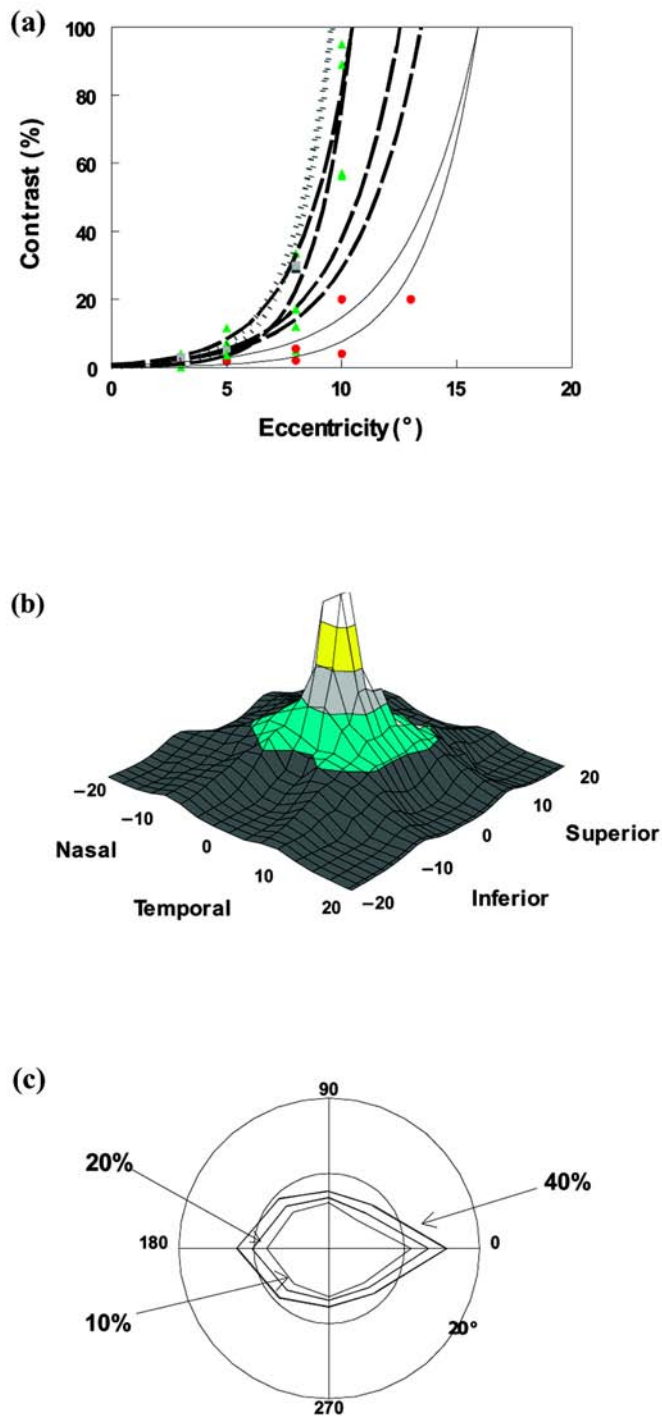


Figure 2.
Grating Acuity. (a) Threshold grating contrast is plotted against eccentricity for 8 meridians: horizontal— 0° and 180° (solid lines/filled circles); vertical— 90° and 270° (broken lines/squares); and oblique— 45° , 135° , 225° , and 315° (dashed lines/triangles). (b) 3D plot of contrast sensitivity ($1/\text{contrast threshold}$) derived from data presented in (a). Lighter areas represent regions with higher sensitivity. (c) Isoacuity plots derived from data presented in (a).

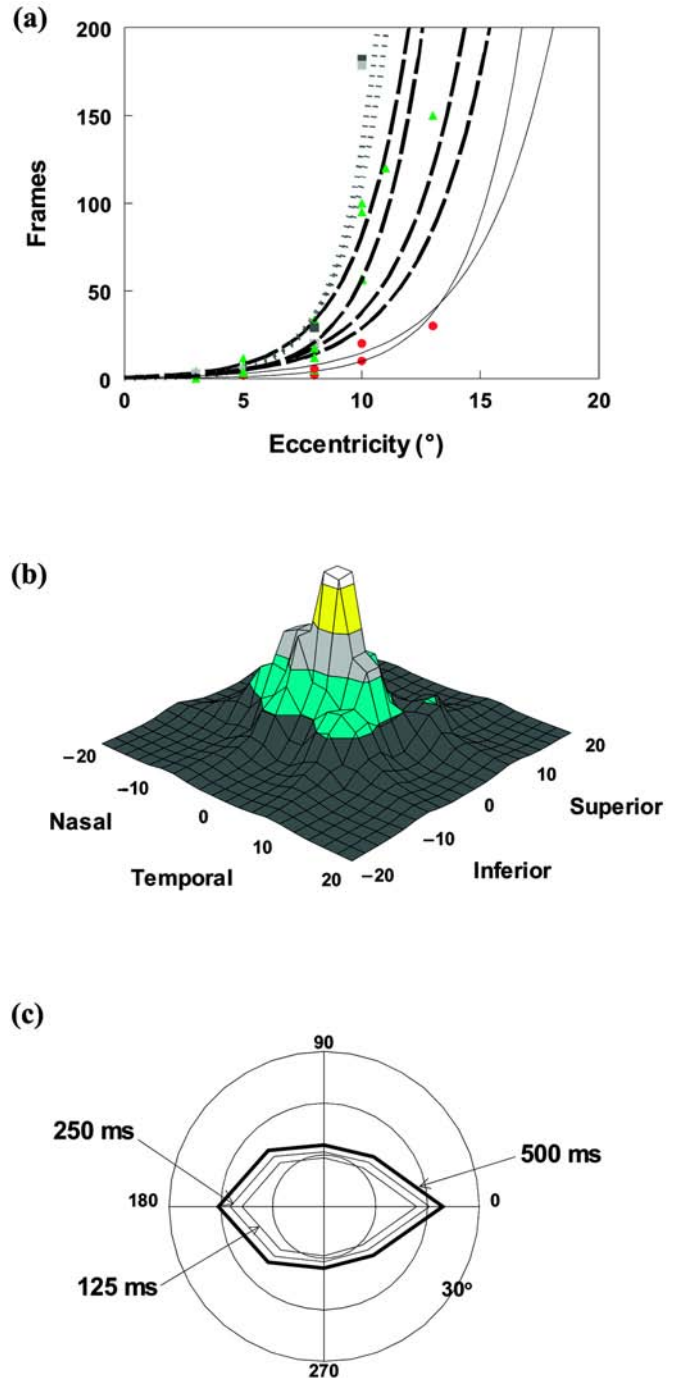


Figure 3.
Duration for Letter Identification. (a) Threshold letter duration is plotted against eccentricity for the 8 meridians: horizontal— 0° and 180° (solid lines/filled circles); vertical— 90° and 270° (broken lines/squares); and oblique— 45° , 135° , 225° , and 315° (dashed lines/triangles). (b) 3D plot of temporal sensitivity ($1/\text{duration threshold}$) derived from data presented in (a). Lighter areas represent regions with higher sensitivity. (c) Isoduration plots derived from data presented in (a).

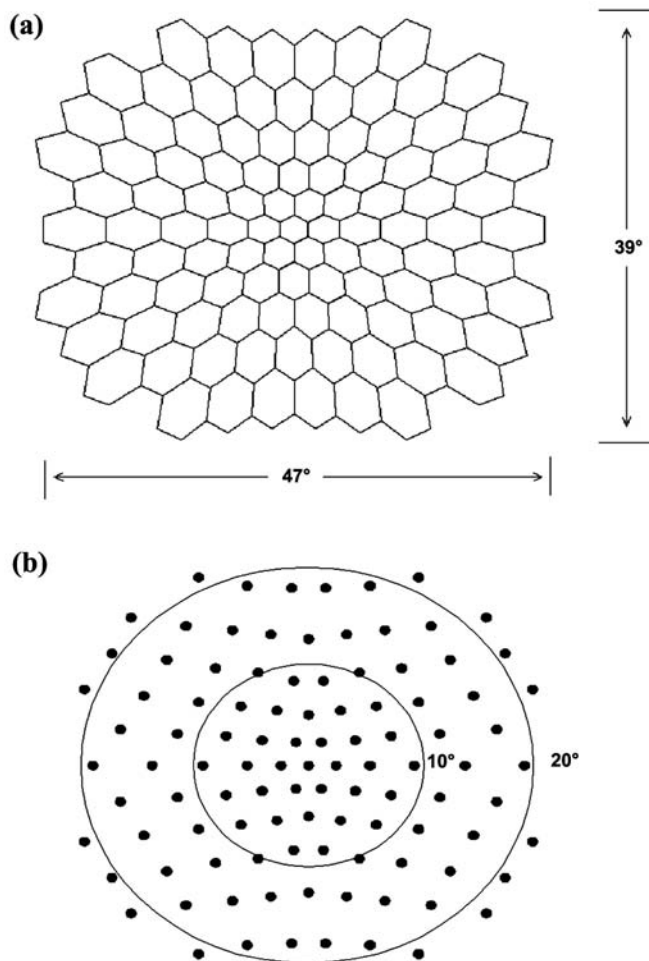


Figure 4.

(a) Hexagon array used to record mfERG. Areas of hexagons were scaled to produce approximately equal amplitude responses at all eccentricities. (b) Positions of test points for the Humphrey visual field. Positions of points were customized to be located at retinal areas corresponding to centers of hexagons in mfERG array.

Experiment IV. Multifocal Electroretinogram

Procedures

The hexagon array used in the mfERG recordings is shown in **Figure 4(a)**, and typical mfERG waveforms are shown in **Figure 5(a)**. Amplitude was measured from the first negative deflection (N1) to the next positive peak (P1) as response density ($\eta v/\sigma^2$).

Results

The median ($N = 4$) mfERG amplitudes are plotted as a function of eccentricity for each meridian in **Figure 6(a)**. The data have been plotted as $1/\text{amplitude}$ to

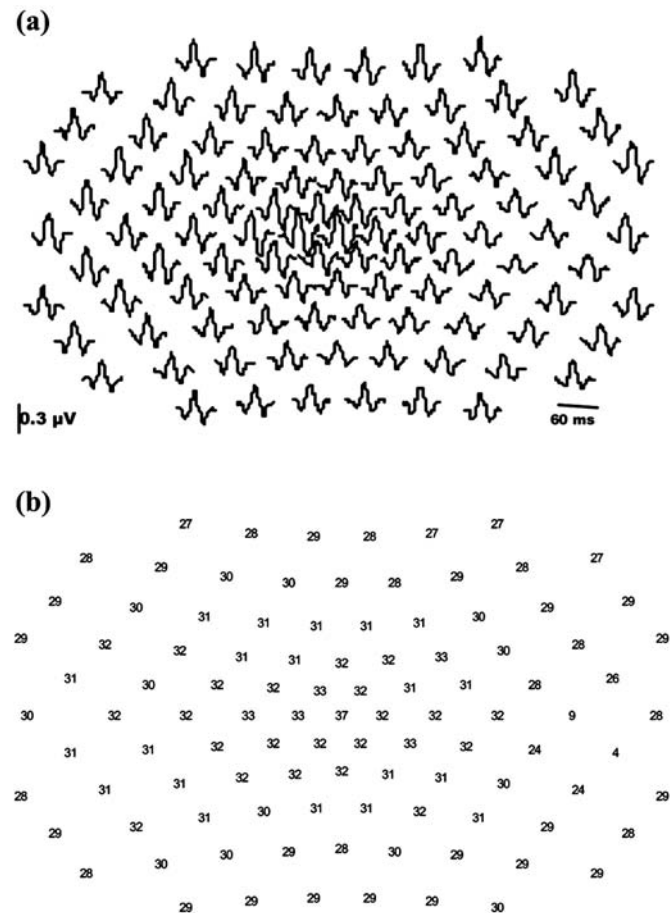


Figure 5.

(a) Representative mfERG waveforms are shown for one subject. (b) Representative Humphrey thresholds (in decibels) are shown for one subject.

make the plot comparable to the psychophysical data (**Figures 1–3**). For all eight meridians, the mfERG amplitude decreased with increasing eccentricity. The rates of amplitude loss along the horizontal and oblique meridians were smaller than along the vertical meridians. The data for each meridian were fitted by equation (1), and the values of these fits are presented in **Table 1**. The average value of A_1 was 0.0085 for the mfERG data. The data were used to plot a 3D map of amplitude (**Figure 6(b)**). MfERG response amplitude peaked at the center, and the rate of amplitude loss as a function of eccentricity was not symmetrical as a function of meridian, showing higher amplitudes along the horizontal than along the vertical meridians at equivalent eccentricities. In **Figure 6(c)**, we plotted the range of eccentricities and the variations with meridian over which mfERG response densities of at least

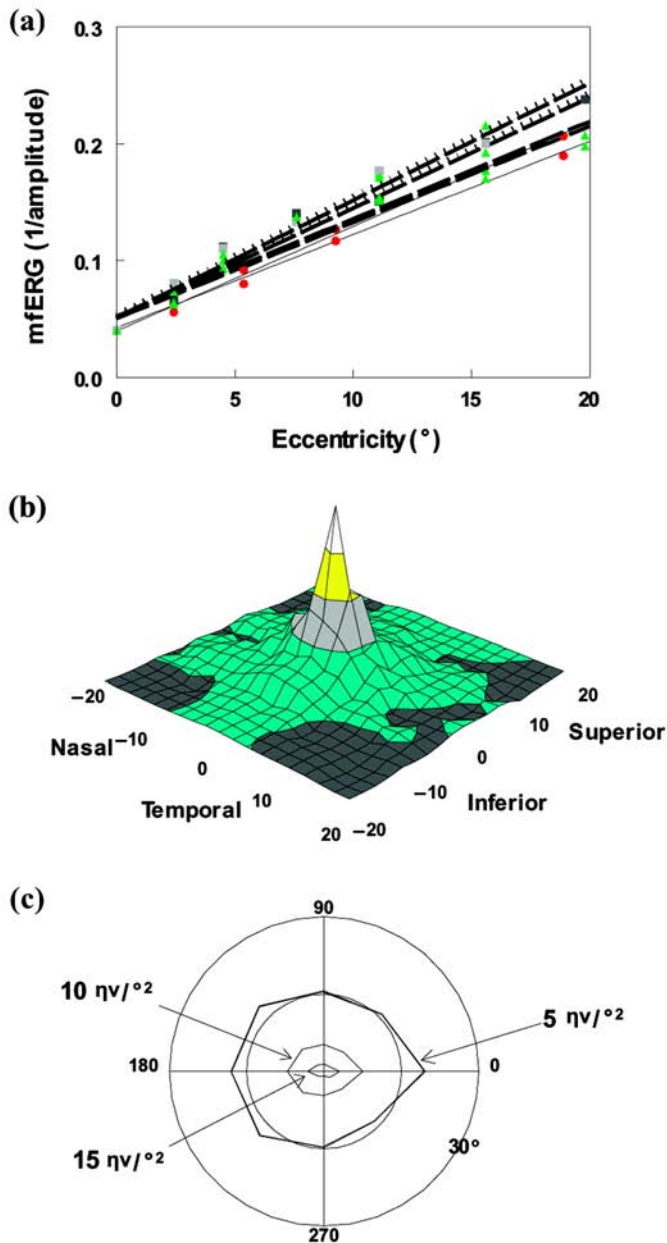


Figure 6. **mfERG Amplitude.** (a) Median ($N = 4$) reciprocal of mfERG amplitudes is plotted against eccentricity for 8 meridians: horizontal— 0° and 180° (solid lines/filled circles); vertical— 90° and 270° (broken lines/squares); and oblique— 45° , 135° , 225° , and 315° (dashed lines/triangles). (b) 3D plot of amplitude derived from data presented in (a). Lighter areas represent regions with higher amplitude. (c) Isoamplitude plots derived from data presented in (a).

a given amplitude (1, 5, 10, and $15 \eta v / \text{°}^2$) can be measured. As the criterion amplitude increased, the range of eccentricities over which responses of this amplitude or

higher was recorded decreased. For example, responses of at least $5 \eta v / \text{°}^2$ were recorded to approximately 18° horizontally and approximately 16° vertically, but responses of at least $15 \eta v / \text{°}^2$ were recorded only to approximately 3° horizontally and approximately 1° vertically.

Experiment V. Humphrey Visual Field Thresholds

Procedures

The locations of the 103 customized points are shown in **Figure 4(b)**. The median ($N = 4$) thresholds in decibels of these 103 points from the Humphrey visual field are shown in **Figure 5(b)**.

Results

The median ($N = 4$) threshold intensities in apostilbs (asbs) are plotted as a function of eccentricity for each meridian in **Figure 7(a)**. For all eight meridians, the threshold decreased with increasing eccentricity. The rate of luminance sensitivity loss as a function of eccentricity was relatively equivalent along all meridians. The data for each meridian were fitted by equation (1). The values of these fits are presented in **Table 1**. Sensitivity peaked at fixation and showed a shallow fall-off with eccentricity, with A_1 averaging 0.01 across all meridians.

The thresholds for all 103 points were used to plot a 3D map of sensitivity as a function of eccentricity and meridian. The results are presented in **Figure 7(b)**. Sensitivity peaked at the center and demonstrated a shallow fall-off with eccentricity. However, the rate of amplitude loss was not symmetrical as a function of meridian, showing higher sensitivities along the horizontal inferior and nasal meridians than along the other meridians. This rate of amplitude loss is shown in the isoamplitude contour plot (**Figure 7(c)**). This plot demonstrates the range of eccentricities and the variations with meridian over which spots of a given intensity (5, 10, and 30 asbs) were detected. As the intensity of the test spot increased, the range of eccentricities over which it was detected also increased.

Correlations Among Measures

The data were converted to the same unit to quantify the retinotopic relationship among measures—logarithm loss from the foveal value was calculated for each measure. Linear regressions were performed on corresponding eccentricity and meridian data. The scatter plots of these comparisons are presented in **Figure 8**; the best-fit

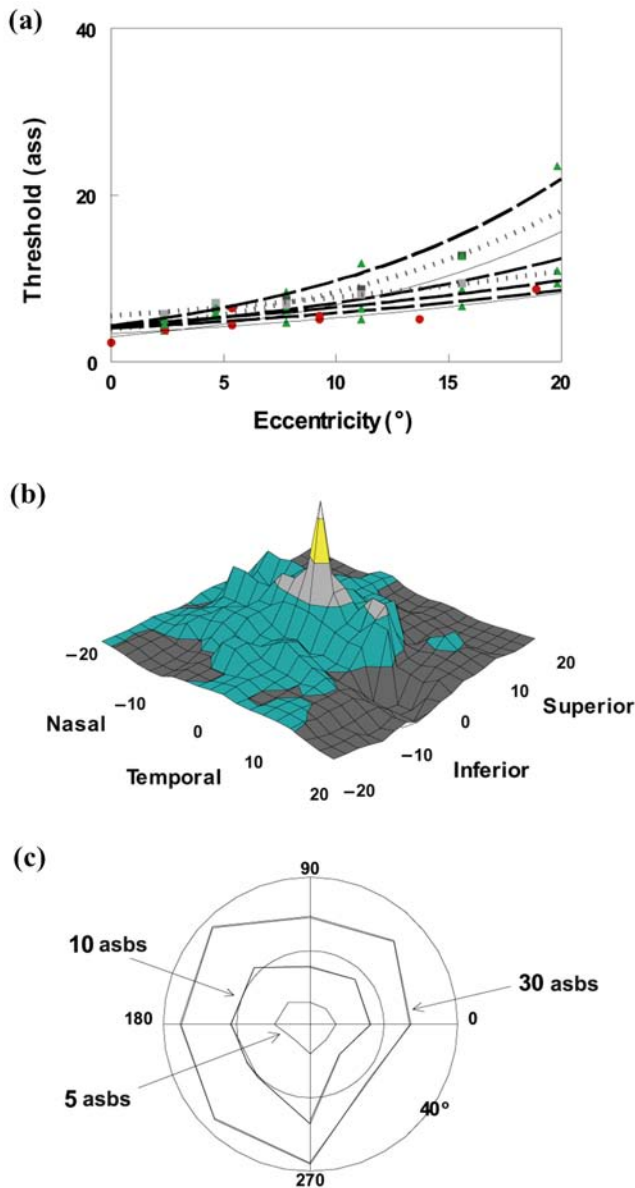


Figure 7. **Humphrey Visual Field Thresholds.** (a) Median ($N = 4$) threshold intensities (in apostilbs) plotted against eccentricity for 8 meridians: horizontal— 0° and 180° (solid lines/filled circles); vertical— 90° and 270° (broken lines/squares); and oblique— 45° , 135° , 225° , and 315° (dashed lines/triangles). (b) 3D plot of sensitivity ($1/\text{threshold}$) derived from the data presented in (a). Lighter areas represent regions with higher sensitivity. (c) Isosensitivity plots derived from data presented in (a).

linear regressions to the data are shown as the solid line in each plot. The fit parameters are presented in **Table 2**. The correlations between acuity and contrast, and between duration for letter identification and mfERG

amplitude were high, whereas the correlations between the Humphrey sensitivity and all other measures were low. From the slopes of these fits, it can be seen that duration sensitivity for letter identification demonstrated the steepest decline with eccentricity among all the measures (note the scale for letter identification data in **Figure 8**).

Correlations with Cone and Ganglion Cell Density

The psychophysical and electrophysiological data were also compared to human cone and ganglion cell density data derived from Curcio et al. [24–26]. The scatter plots of these comparisons are presented in **Figure 9**. For each comparison, the data from the more central locations appear in the lower left and the data from the more peripheral locations appear in the upper right. The best-fit linear regressions to all the data are shown as the dotted lines. The fit parameters are presented in **Table 3**. All measures showed statistically significant correlations with the anatomical data. Acuity and contrast sensitivity had the highest correlation coefficients with the anatomical data, whereas the Humphrey thresholds had the lowest correlation coefficients. When the data were examined separately for points $<10^\circ$ (filled circles) and $>10^\circ$ (open circles), the slopes were shallower for the more eccentric points than for the centermost points (**Figure 9**). The mfERG data were exceptions to these measurement results.

CONCLUSIONS

We have demonstrated that acuity, contrast sensitivity, and temporal sensitivity for letter identification decrease as a function of retinal eccentricity for all meridians. These findings parallel the reports of many studies. Acuity [27,28], contrast sensitivity [9,29,30], temporal frequency [12,17,31,32], flicker adaptation [33], light adaptation [34,35], texture discrimination [22,36,37], and ERG temporal properties [17] vary with eccentricity. The losses of psychophysical sensitivity as a function of eccentricity have been related to decreases in cone and ganglion cell density [24,26,27,38–40], changes in cone morphology [12], increases in ganglion cell receptive field size [41], and decreases in cortical representation as a function of increased eccentricity [9].

Perhaps of greater interest is our finding that the rate of sensitivity loss within each measure varied as a function of meridian. In general, sensitivity was maintained in the horizontal meridians to a greater extent than in the

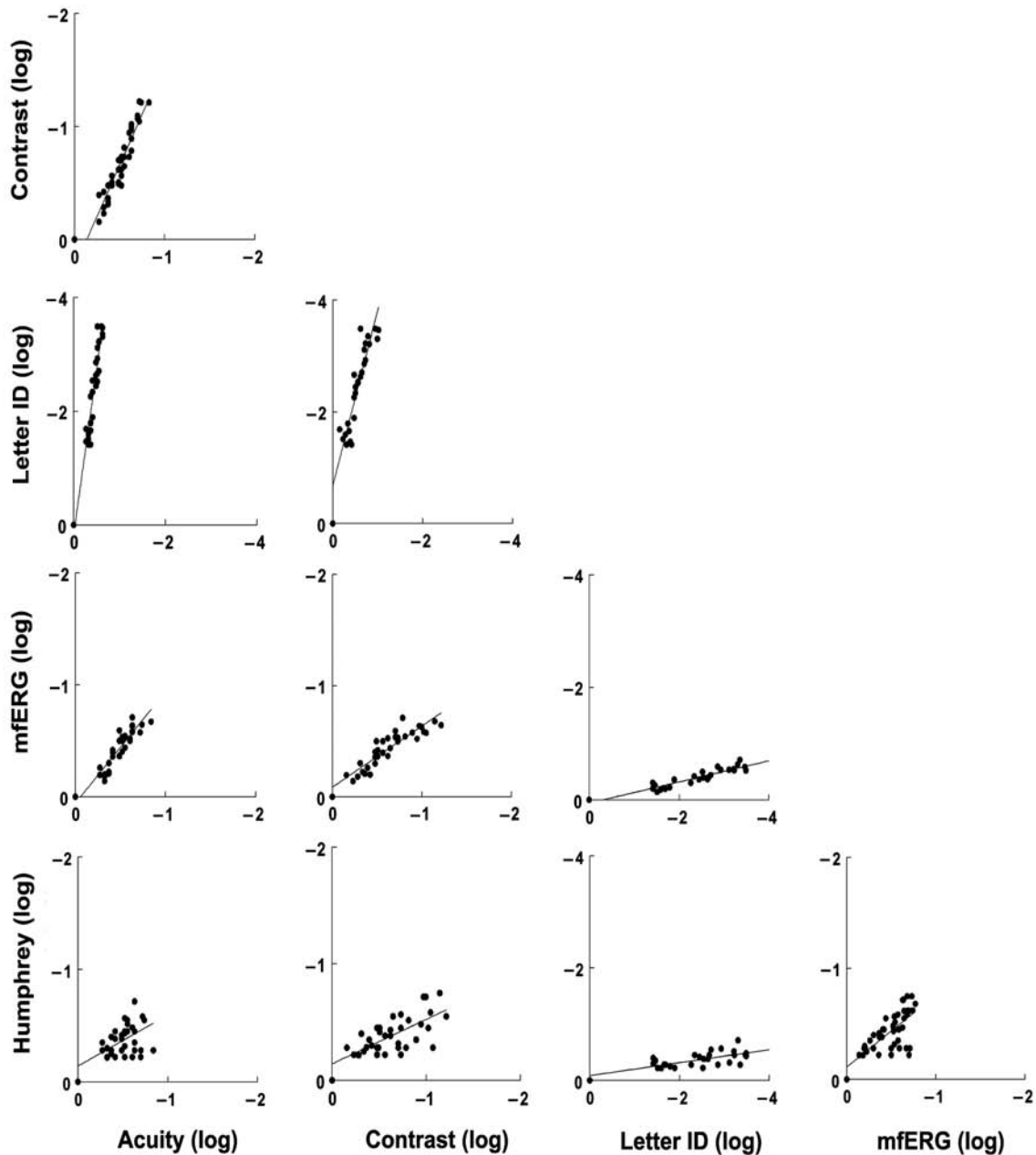


Figure 8.

Correlations. For each plot, log loss from the fovea value for a given measure was plotted against log loss from the fovea value for the other measure for equivalent eccentricities and meridians. Lines through data are derived from best-fit regressions. Statistics of regression fits are presented in **Table 2**.

vertical meridians. This is consistent with previous psychophysical studies [38]. Rovamo et al. [19] reported that the resolution of large sinusoidal gratings presented for a relatively long duration (500 ms) depended upon eccentricity and meridian. However, this dependence was

strongly influenced by grating orientation. Regan and Beverley [18] measured contrast sensitivity for counter-phase modulated (8 Hz) sine wave gratings and found that the contrast sensitivity of locations along the horizontal meridian was higher than corresponding eccentricities

Table 2.
Regression results (all measures). ID = identification.

<i>x</i>	<i>y</i>	Slope	<i>r</i>	<i>p</i>
Acuity	Humphrey	0.45	0.50	<0.001
	mfERG	1.00	0.91	0.002
	Letter ID	5.80	0.95	<0.001
	Contrast	1.80	0.94	<0.001
Contrast	Humphrey	0.38	0.69	<0.001
	mfERG	0.55	0.91	<0.001
	Letter ID	3.15	0.84	<0.001
Letter ID	Humphrey	0.12	0.69	<0.001
	mfERG	0.19	0.93	0.005
mfERG	Humphrey	0.65	0.70	<0.001

along the vertical and oblique meridians. Rijdsdijk et al. [42] reported similar contrast threshold findings for complex 2-D gratings modulated sinusoidally in both horizontal and vertical directions. Van de Gind et al. [43] reported inhomogeneities for motion detection, with thresholds for targets in the vertical meridian higher than thresholds for targets in the horizontal meridian.

More recently, Mackeben [20] reported a meridian dependence for letter recognition in a sustained attention task. These differences in electrophysiological and psychophysical function parallel the distribution of retinal elements. Curcio et al. [24] reported that the cone density was highest along the horizontal meridian and that the cone density in the superior retina exceeded that in the inferior retina. Likewise, ganglion cell densities also followed the same distribution pattern. Curcio and Allen [26] suggested that the lines of isoacuity resemble more closely the distribution of ganglion cells than those of the cone photoreceptors. Indeed, there have been reports of linear relationships between acuity and ganglion cell separation when measured beyond 10° of eccentricity [44,45].

At more central locations in the visual field, relationships with ganglion cell anatomy are more complex, because of foveal excavation and subsequent lateral displacement of ganglion cells and because central cone photoreceptors may diverge to two or three ganglion cells [26, 46]. In the central retina, but not beyond 10° due to convergence, direct relationships between cone density and acuity have been demonstrated [45,47–51].

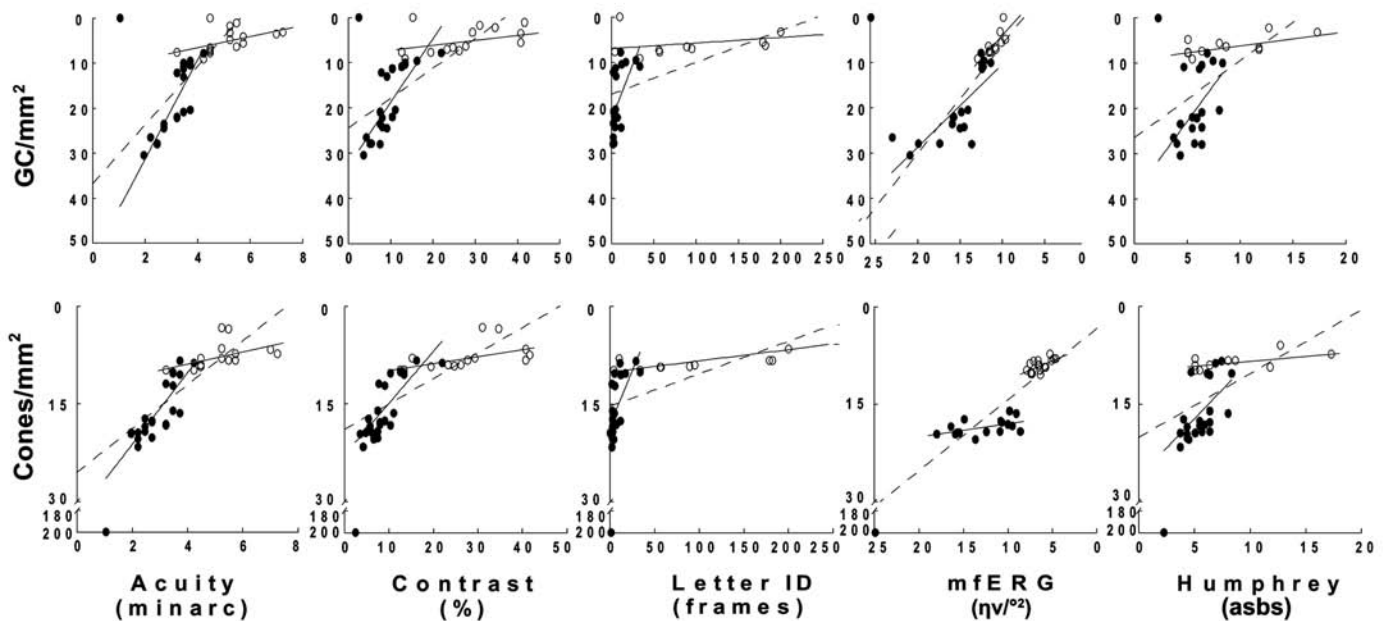


Figure 9.

Cone and Ganglion Cell Density. Threshold values for each measure are plotted against corresponding anatomical data for each position on the retina. **Top Row:** Data plotted against ganglion cell densities. **Bottom Row:** Data plotted against cone densities. Lines through data are derived from best-fit regressions. Statistics of regression fits are presented in Table 3. Filled circles = points < 10°, open circles = points > 10°.

Table 3.

Regression results (with anatomic measures). ID = identification.

<i>x</i>	<i>y</i>	All Slope	<i>r</i>	<i>p</i>	<10° Slope	<i>r</i>	<i>p</i>	>10° Slope	<i>r</i>	<i>p</i>
Cone	Acuity	-3.37	0.85	<0.001	-5.50	0.84	<0.001	-0.93	0.48	0.060
	Contrast	-0.39	0.82	<0.001	-0.82	0.81	<0.001	-0.11	0.53	0.050
	Letter ID	-0.05	0.65	<0.001	-0.33	0.67	<0.001	-0.02	0.78	0.005
	mfERG	1.09	0.86	<0.001	0.20	0.51	0.045	0.60	0.63	0.007
	Humphrey	-1.01	0.58	<0.001	-1.97	0.61	0.002	-0.16	0.55	0.080
Ganglion	Acuity	-6.52	0.84	<0.001	-11.02	0.87	<0.001	-1.23	0.44	0.130
	Contrast	-0.66	0.79	<0.001	-1.41	0.81	<0.001	-0.14	0.47	0.090
	Letter ID	-0.07	0.59	<0.001	-0.46	0.59	0.010	-0.01	0.37	0.260
	mfERG	2.41	0.87	<0.001	1.83	0.78	<0.001	2.06	0.78	0.005
	Humphrey	-1.70	0.56	0.002	-3.22	0.55	0.017	-0.340	0.67	0.025

In **Figures 8** and **9**, we examined the relationships between psychophysical and electrophysiological measures and between these measures and cone or ganglion cell density (derived from Curcio et al. [24,26]). We found that, for most measures, the slope of the relationship at <10° was steeper from that at >10°. This was especially true for the mfERG comparisons, where the slope of the fit to the data >10° approached zero. For the Humphrey visual field data, the slopes of the two comparisons were similar.

These maps and the correlations among measures as a function of retinal position serve as a baseline so that we can examine disease effects throughout the retina. In addition, the development of vision rehabilitation programs should take into account the differential sensitivities of the peripheral retina. For example, our finding that temporal sensitivity demonstrates a steep decline with eccentricity suggests that programs attempting to train patients to use eccentric locations for reading rehabilitation should account for target duration, as well as magnification in letter size.

REFERENCES

1. Sutter EE, Tran D. The field topography of ERG components in man. Part I: The photopic luminance response. *Vision Res.* 1992;32(3):433–46.
2. Hood DC. Assessing retinal function with the multifocal technique. *Prog Ret Eye Res.* 2000;19(5):607–46.
3. Sutter EE. Imaging visual function with the multifocal m-sequence technique. *Vision Res.* 2001;41(10–11):1241–55.
4. Alexander KR, Xie W, Derlacki DJ, Szlyk JP. Effect of spatial sampling on grating resolution and letter identification. *J Opt Soc Am A Opt Image Sci Vis.* 1995;12(9):1825–33.
5. Geller AM, Sieving PA, Green DG. Effect on grating identification of sampling with degenerate arrays. *J Opt Soc Am A Opt Image Sci Vis.* 1992;9(3):472–77.
6. Seiple W, Holopigian K, Szlyk JP, Greenstein VC. The effects of random element loss on letter identification: implications for visual acuity loss in patients with retinitis pigmentosa. *Vision Res.* 1995;35(14):2057–66.
7. Seiple W, Greenstein VC, Holopigian K, Carr RE, Hood DC. A method for comparing psychophysical and multifocal electroretinographic increment thresholds. *Vision Res.* 2002;42:257–69.
8. Rovamo J, Virsu V. An estimation and application of the human cortical magnification factor. *Exp Brain Res.* 1979; 37(3):495–510.
9. Virsu V, Rovamo J. Visual resolution, contrast sensitivity, and the cortical magnification factor. *Exp Brain Res.* 1979; 37(3):475–94.
10. Westheimer G. Temporal order detection for foveal and peripheral visual stimuli. *Vision Res.* 1983;23(8):759–63.
11. Douthwaite WA, Halliwell JA, Lomas AM, Yan Muk WK, Topliss JN. Critical fusion frequency in the central visual field. *Ophthalmic Physiol Opt.* 1985;5(1):15–21.
12. Tyler CW. Analysis of visual modulation sensitivity. II. Peripheral retina and the role of photoreceptor dimensions. *J Opt Soc Am A Opt Image Sci Vis.* 1985;(2):393–98.
13. Tyler CW. Analysis of visual modulation sensitivity. III. Meridional variations in peripheral flicker sensitivity. *J Opt Soc Am A Opt Image Sci Vis.* 1987;4:1612–19.
14. Raninen A, Rovamo J. Perimetry of critical flicker frequency in human rod and cone vision. *Vision Res.* 1986;26(8):1249–55.
15. Raninen A, Franssila R, Rovamo J. Critical flicker frequency to red targets as a function of luminance and flux across the human visual field. *Vision Res.* 1991;31(11):1875–81.

16. Seiple W, Holopigian K, Greenstein VC, Hood DC. Temporal frequency dependent adaptation at the level of the outer retina in humans. *Vision Res.* 1992;32(11):2043–48.
17. Seiple W, Holopigian K. Outer-retina locus of increased flicker sensitivity of the peripheral retina. *J Opt Soc Am A Opt Image Sci Vis.* 1996;13(3):658–66.
18. Regan D, Beverley K I. Visual fields described by contrast sensitivity, by acuity, and by relative sensitivity to different orientations. *Invest Ophthalmol Vis Sci.* 1983;24(6):754–59.
19. Rovamo J, Virsu V, Laurinen P, Hyvarinen L. Resolution of gratings oriented along and across meridians in peripheral vision. *Invest Ophthalmol Vis Sci.* 1982;23(5):666–70.
20. Mackeben M. Sustained focal attention and peripheral letter recognition. *Spat Vis.* 1999;12(1):51–72.
21. Wolf AM, Gaeta M, Geer SE. Critical flicker frequencies in flicker perception. *Arch Ophthalmol.* 1968;80:347–51.
22. Seiple W, Holopigian K, Shnayder Y, Szlyk JP. Duration thresholds for target detection and identification in the peripheral visual field. *Optom Vis Sci.* 2001;78(3):169–76.
23. Hood DC, Seiple W, Holopigian K, Greenstein VC. A comparison of the components of the multifocal and full-field ERGs. *Vis Neurosci.* 1997;14(3):533–44.
24. Curcio CA, Sloan KR, Kalina RE, Hendrickson AE. Human photoreceptor topography. *J Comp Neurol.* 1990;292(4):497–523.
25. Curcio CA, Sloan KR. Packing geometry of human cone photoreceptors: variation with eccentricity and evidence for local anisotropy. *Vis Neurosci.* 1992;9(2):169–80.
26. Curcio CA, Allen KA. Topography of ganglion cells in human retina. *J Comp Neurol.* 1990;300(1):5–25.
27. Cowey A, Rolls ET. Human cortical magnification factor and its relation to visual acuity. *Exp Brain Res.* 1974;21(5):447–54.
28. Drasdo N. The neural representation of visual space. *Nature.* 1977;266(5602):554–56.
29. Koenderink JJ, Bouman MA, Bueno de Mesquita AE, Slappendel S. Perimetry of contrast detection thresholds of moving spatial sine wave patterns. Part I: The near peripheral visual field (eccentricity 0 degrees–8 degrees). *J Opt Soc Am.* 1978;68(6):845–49.
30. Navarro R, Artal P, Williams DR. Modulation transfer of the human eye as a function of retinal eccentricity. *J Opt Soc Am A Opt Image Sci Vis.* 1993;10(2):201–12.
31. McKee SP, Taylor DG. Discrimination of time: comparison of foveal and peripheral sensitivity. *J Opt Soc Am A Opt Image Sci Vis.* 1984;1(6):620–27.
32. Virsu V, Rovamo J, Laurinen P, Nasanen R. Temporal contrast sensitivity and cortical magnification. *Vision Res.* 1982;22(9):1211–17.
33. Schieting S, Spillmann L. Flicker adaptation in the peripheral retina. *Vision Res.* 1987;27(2):277–84.
34. Rovamo J, Raninen A. Cortical acuity and the luminous flux collected by retinal ganglion cells at various eccentricities in human rod and cone vision. *Vision Res.* 1990;30(1):11–21.
35. Tyler CW, Hamer RD. Analysis of visual modulation sensitivity. Part IV: Validity of the Ferry-Porter law. *J Opt Soc Am A Opt Image Sci Vis.* 1990;7(4):743–58.
36. Saarinen J, Rovamo J, Virsu V. Analysis of spatial structure in eccentric vision. *Invest Ophthalmol Vis Sci.* 1989;30(2):293–96.
37. Szlyk JP, Seiple W, Xie W. Symmetry discrimination in patients with retinitis pigmentosa. *Vision Res.* 1995;35(11):1633–40.
38. Weymouth FW. Visual sensory units and minimum angle of resolution. *Am J Ophthalmol.* 1958;46:102–13.
39. Osterberg G. Topography of the layer of rods and cones in the human retina. *Acta Ophthalmol Scand Suppl.* 1935;6:1–103.
40. Sjostrand J, Popovic Z, Conradi N, Marshall J. Morphometric study of the displacement of retinal ganglion cells subserving cones within the human fovea. *Graefes Arch Clin Exp Ophthalmol.* 1999;237(12):1014–23.
41. Rovamo J, Raninen A, Virsu V. The role of retinal ganglion cell density and receptive-field size in photopic perimetry. In: Greve EL, Heijl A, editors. *Proceedings of the 6th International Visual Field Symposium; 1985 May 27–31; Santa Margherita, IT. The Netherlands: W. Junk; 1985. p. 589–93.*
42. Rijdsdijk JP, Kroon JN, van der Wildt GJ. Contrast sensitivity as a function of position on the retina. *Vision Res.* 1980;20:235–41.
43. van de Gind WA, Koenderink JJ, van Dorn AJ, Milders MV, Voerman H. Inhomogeneity and anisotropies for motion detection in the monocular visual field of human observers. *Vision Res.* 1993;33(8):1089–107.
44. Frisen L. High-pass resolution targets in peripheral vision. *Ophthalmology.* 1987;94(9):1104–08.
45. Merigan W H, Katz L M. Spatial resolution across the macaque retina. *Vision Res.* 1990;30(7):985–91.
46. Sjostrand J, Olsson V, Popovic Z, Conradi N. Quantitative estimations of foveal and extra-foveal retinal circuitry in humans. *Vision Res.* 1999;39(18):2987–98.
47. Hirsch J, Curcio CA. The spatial resolution capacity of human foveal retina. *Vision Res.* 1989;29(9):1095–101.
48. Coletta NJ, Williams DR. Psychophysical estimate of extrafoveal cone spacing. *J Opt Soc Am A Opt Image Sci Vis.* 1987;4(8):1503–13.
49. Thibos LN, Cheney FE, Walsh DJ. Retinal limits to the detection and resolution of gratings. *J Opt Soc Am A Opt Image Sci Vis.* 1987;4(8):1524–29.
50. Frisen L. High-pass resolution perimetry: central-field neuroretinal correlates. *Vision Res.* 1995;35(2):293–301.
51. Rolls ET, Cowey A. Topography of the retina and striate cortex and its relationship to visual acuity in rhesus monkeys and squirrel monkeys. *Exp Brain Res.* 1970;10(3):298–310.

Submitted for publication July 21, 2003. Accepted in revised form November 13, 2003.